



Coseismic Fault Slip of the September 16, 2015 M_w 8.3 Illapel, Chile Earthquake Estimated from InSAR Data

YINGFENG ZHANG,^{1,2} GUOHONG ZHANG,¹ ERIC A. HETLAND,³ XINJIAN SHAN,¹ SHAOYAN WEN,^{1,4} and RONGHU ZUO¹

Abstract—The complete surface deformation of 2015 M_w 8.3 Illapel, Chile earthquake is obtained using SAR interferograms obtained for descending and ascending Sentinel-1 orbits. We find that the Illapel event is predominantly thrust, as expected for an earthquake on the interface between the Nazca and South America plates, with a slight right-lateral strike slip component. The maximum thrust-slip and right-lateral strike slip reach 8.3 and 1.5 m, respectively, both located at a depth of 8 km, northwest to the epicenter. The total estimated seismic moment is 3.28×10^{21} N.m, corresponding to a moment magnitude M_w 8.27. In our model, the rupture breaks all the way up to the sea-floor at the trench, which is consistent with the destructive tsunami following the earthquake. We also find the slip distribution correlates closely with previous estimates of interseismic locking distribution. We argue that positive coulomb stress changes caused by the Illapel earthquake may favor earthquakes on the extensional faults in this area. Finally, based on our inferred coseismic slip model and coulomb stress calculation, we envision that the subduction interface that last slipped in the 1922 M_w 8.4 Vallenar earthquake might be near the upper end of its seismic quiescence, and the earthquake potential in this region is urgent.

Key words: The 2015 Illapel earthquake, InSAR displacement, coseismic slip model, faults reactivation, coulomb stress change.

1. Introduction

On 16 September 2015, an M_w 8.3 earthquake occurred with epicenter to the west of Illapel, Chile, the first megathrust earthquake in central Chile since the 2010 M_w 8.8 Maule earthquake. This earthquake ruptured the Coquimbo seismic gap that has been monitored with a dense space-geodetic network (VIGNY *et al.* 2011). This earthquake resulted in a severe tsunami with run-up as high as 4.5 m (CONTRERAS-LÓPEZ *et al.* 2016), which struck the Chilean coastal cities and resulted in heavy damage, especially to Socos beach, a famous tourist spot. The earthquake was followed by many large aftershocks, including two $>M_w$ 6.5 on 17 and 21 September. All of the aftershocks for which focal mechanisms were determined are thrust events with gentle dips, similar to the main shock, indicating thrust motion on the subduction interface in Central Chile.

Based on hypocentral location and focal mechanism solution, the Illapel earthquake occurred along the collision zone between the Nazca and South American Plate that converge at a rate of 8 cm year^{-1} in the N78°E direction (DE METS *et al.* 1990). Its tectonic setting is characterized by slightly dextral-oblique convergence between the Nazca and South American Plate margins that has been subducting for the last 20 Ma (Fig. 1; PARDO-CASAS *et al.* 1987; SOMOZA 1998; ANGERMANN *et al.* 1999; CEMBRANO *et al.* 2009). The plate boundary at these latitudes is characterized by a partitioning of deformation with a large number of destructive thrust earthquakes and resulting tsunamis in the subduction zone (BARRIENTOS *et al.* 1990; CISTERNAS *et al.* 2005; WATT *et al.* 2009), such as the recent Maule M_w 8.8 earthquake on February 27, 2010 (VIGNY *et al.* 2011)

Electronic supplementary material The online version of this article (doi:10.1007/s00024-016-1266-3) contains supplementary material, which is available to authorized users.

¹ State Key Laboratory of Earthquake Dynamics, Institute of Geology, China Earthquake Administration, Beijing 100029, China. E-mail: zhanggh@ies.ac.cn

² China University of Petroleum (East China), School of Geoscience, Qingdao 266580, China.

³ Earth and Environmental Sciences, University of Michigan, Ann Arbor 48109, USA.

⁴ Earthquake Administration of Xinjiang, Uygur Autonomous Region, Urumqi 830002, China.

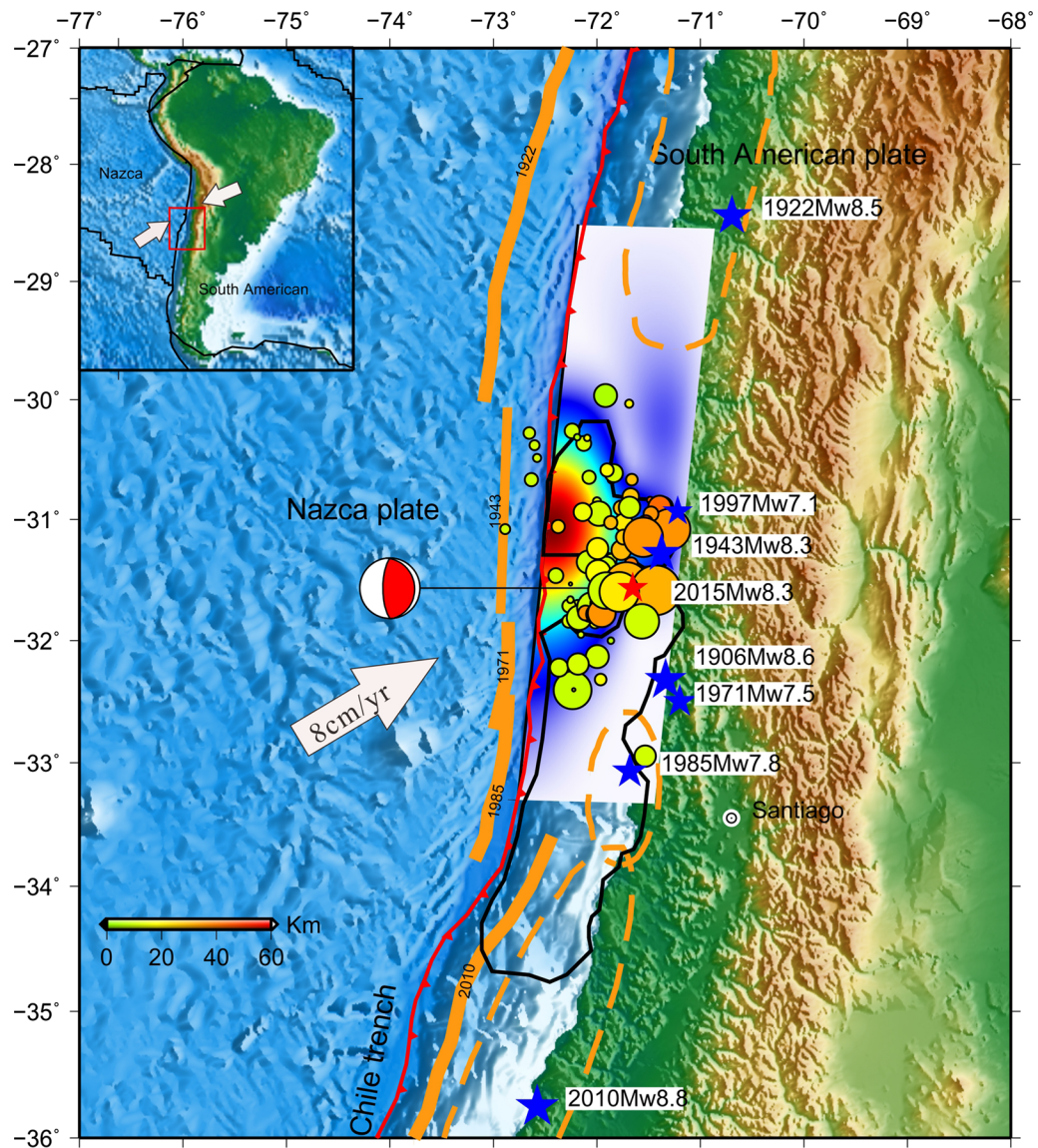


Figure 1

Seismotectonic setting of the Andean Cordillera. Red dots show major historical earthquakes along the Chile Trench, and orange dashed ellipses and orange solid lines are their rupture areas and inferred rupture extends, respectively. Circles present the locations of aftershocks $>M_w 4$ during the following days according to the USGS. The black solid lines present the locking zones. Slip distribution of the Illapel earthquake is also shown, but see more detail in Fig. 3

and the Valdivia Mw 9.5 megathrust earthquake on May 23, 1960 (BARRIENTOS and WARD 1990). The Coquimbo-Illapel area (30° – 32° S) in Northern part of the Central Chile was the site of major earthquakes in 1730, 1880 and 1943 (NISHENKO 1985; BECK *et al.* 1998). The last major event in this area occurred on 15 October 1997 at a depth of 55 km under the city of Punitaqui (PARDO *et al.* 2002). As for this most recent

earthquake, it released east–west compressional strain accumulated in South America by the eastward subducting Nazca Plate.

This event provides another excellent opportunity to study the source parameters of a megathrust earthquake with high-resolution InSAR measurements, and to assess the risk of continued earthquakes in central Chile. We first obtain the coseismic surface

deformation measured through SAR Interferometry (InSAR) of Sentinel-1, using images acquired before and after the Illapel event, which permits a detailed study on the distribution of coseismic fault slip. We invert for a coseismic slip model of the Mw 8.3 Illapel earthquake using this combination of ascending and descending InSAR data. Based on our coseismic fault slip model, we calculate the static Coulomb stress change on two types of representative normal faults to identify whether the main shock has promoted failure of these normal faults, as well as on faults with geometry of the 1922 Mw 8.4 Vallenar earthquake. Finally, we discuss the implications and continued seismic hazards in this area.

2. SAR Data and InSAR Processing

We use six descending Sentinel-1A IW frames and two ascending Sentinel-1A IW frame of SAR images immediately after the event, to extrude post-seismic deformation and aftershocks as possible as we can. The three descending frames belong to the same track, which is sub-parallel to the Chile coast and thus the descending observing mode of the coseismic deformation covers a larger range than the ascending mode, since we obtain only one frame of the ascending SAR images. The SAR data only measures the terrestrial coseismic displacements (Fig. 2). All of the images are processed with the conventional two-pass differential InSAR method using the GAMMA software package (WEGMÜLLER *et al.* 1997; FENG *et al.* 2015). The raw data are transformed into single-look images (SLCs) and then the interferograms are generated through interferometry of the SLC images. We use the SRTM 3 s data to estimate the topographic phases (FARR *et al.* 2000) and remove them from interferograms. We do not estimate corrections to the orbital geometric phases, due to the high precision of Sentinel-1 orbital data. We unwrap the interferograms with the minimum cost flow algorithm (MCF, WERNER *et al.* 2002). Despite the incomplete deformation field, the quality of the InSAR data is excellent and we obtain clear, smooth and continuous interferograms (Fig. 2).

Both the coseismic ascending and descending InSAR measurements reveal that the maximum LOS

displacement on continent is >130 cm about 60 km northwest of hypocenter along the Chile coast. The LOS displacements range from 1 to 132 cm along the ascending orbits and -136 to 3 cm along the descending orbits. The InSAR measurements exhibit strong surface displacements, consistent with an Mw 8.3 earthquake. The interferograms reveal no clear phase discontinuities or surface rupture on the continent in this event.

3. Fault Slip Modeling

Inversion of the full data is not tractable due to the large number of pixels in the interferograms (e.g., SIMONS *et al.* 2002; ZHANG *et al.* 2011). We down-sample the interferograms and get a more manageable data for inversion using a quad-tree sampling method (e.g., SIMONS *et al.* 2002). The total number of LOS measurements that we invert in the descending and the ascending interferograms are about 12,000 and 5000, respectively. In the fault slip modeling, we use a low-angle, anti-listric thrust-slip fault model to approximate the increase of dip of the subduction interface. The fault has a strike of 4° with length and width 520 and 160 km, respectively. Based on trial and error, we find that a fault dip increasing from 15 to 20 degrees along the down-dip direction has the lowest data misfit to the InSAR data. The fault geometry is consistent with the finite fault solution of YE *et al.* (2015), as well as coseismic models of previous earthquakes on this subduction boundary (e.g., DELOUIS *et al.* 2010; TONG *et al.* 2010; POLLITZ *et al.* 2011). To determine a finer slip distribution, the fault plane is further discretized into 10 km \times 10 km fault patches and we solve for static fault slip on each patch.

We invert the sub-sampled InSAR measurements, denoted with the vector d , using a constrained least-square method of WANG *et al.* (2003) which finds a slip model, s , that minimized

$$f(s) = \|d - d_0 - Gs\|^2 + \beta^2 \|Hs\|^2, \quad (1)$$

where G is the Green's function matrix calculated using slip on a fault in a homogeneous elastic half-space (OKADA 1992), assuming a Poisson ratio of

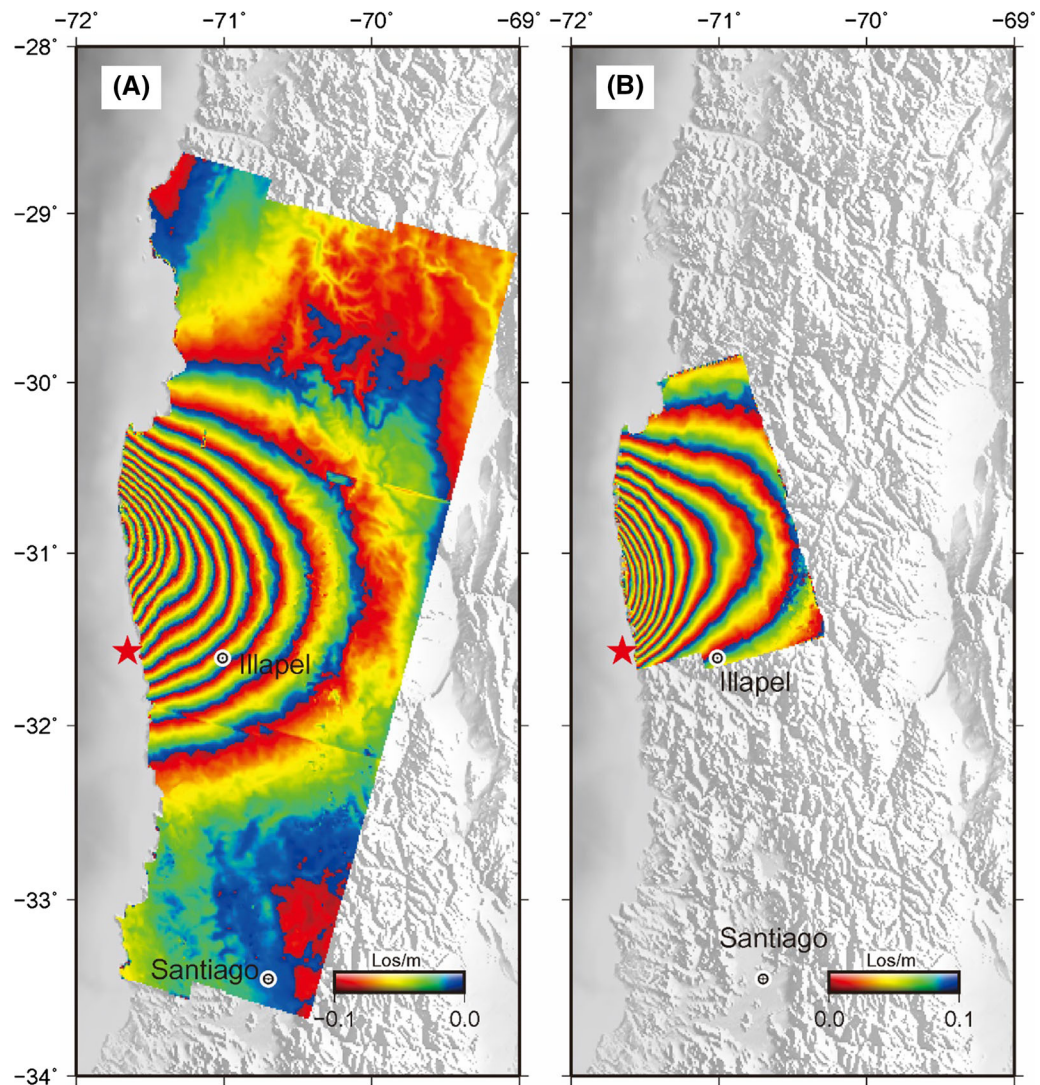


Figure 2

Interferograms of M_w 8.3 Illapel earthquake. *Left* the descending interferogram detected by Sentinel-1 SAR data. *Right* the ascending Interferogram by Sentinel-1 SAR data. Each color cycle represents 10.0 cm line-of-sight (LOS) displacement

0.25, which describes the relation between the model prediction and InSAR measurement. Because each of the interferograms has a unique starting position for the unwrapping algorithm, there is an unknown constant offset in LOS displacement associated with each of the interferograms. To account for this ambiguity, we include an offset for each of the InSAR interferograms d_0 . The inversion is regularized using a Laplacian smoothness constraint on fault slip, where β^2 represents the smoothing factor, H is the Laplacian operator, and $\|Hs\|$ represents a

measure of the slip roughness. The smoothing factor can balance the roughness of fault slip and the data misfit. In this study, the L-curve method is utilized to choose an optimal smoothing factor, which we find to be 0.1 (e.g., HANSEN 1992; FENG *et al.* 2012, 2015; ZHANG *et al.* 2011). Additionally, we constrain the slip rake in each sub-fault within 80° – 150° based on historical events mechanisms (where 90° is pure thrust slip). We equally weight both of the ascending and descending InSAR measurements in the inversion.

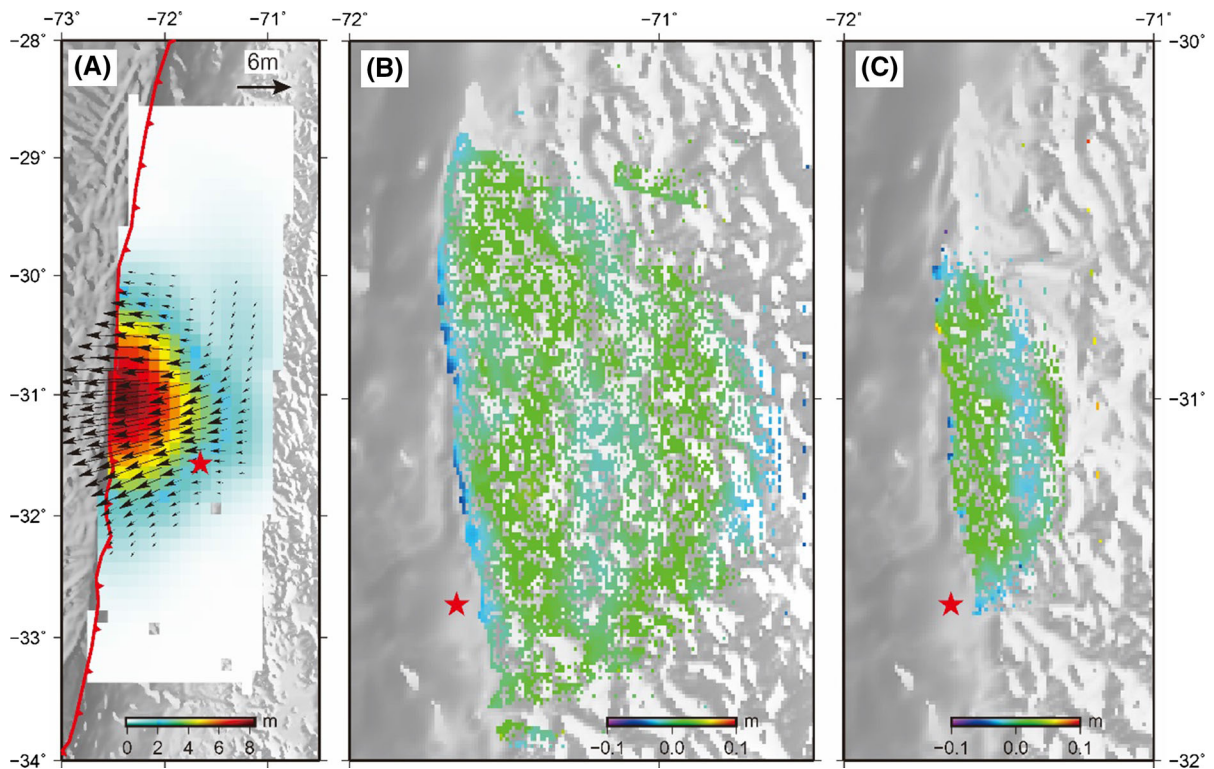


Figure 3

Fault slip distributions of M_w 8.3 Illapel earthquake and InSAR data residuals from optimal inversion. **b**, **c** Present the descending and ascending residuals, respectively

The slip distribution and its corresponding fit to InSAR data are shown in Fig. 3. The residuals of InSAR LOS displacement are generally smaller than 4 cm away from the coast, although the misfit to the LOS measurements in near the coast are larger, likely due to the having no constraint of InSAR data in the sea (Fig. 3). The average RMS for measurements from the ascending and descending interferograms is about 1.7 cm and about 1.5 cm, respectively. The coseismic slip model reveals primarily reverse fault motion, as expected for this region and from the focal mechanism solutions, with a small component of right lateral strike slip. The maximum thrust slip of 8.3 m at a depth of 1.5 km northwest to the epicenter and the maximum of 1.5 m right-lateral strike slip at the same depth but slightly closer to the epicenter. Because of lack of observations offshore that contain most of the near field data, the geodetic model probably underestimates the amount of slip at shallower depth. Comparing to the finite-fault models

inverted from broadband waveforms (e.g., YE *et al.* 2015; http://earthquake.usgs.gov/earthquakes/eventpage/us20003k7a-scientific_finitefault), we find that the maximum slip (about 9.0 m) and rupture zone are similar with our slip model derived from InSAR data. However, our model is more compact and smooth than the results of broadband waveforms, due to different damping strategies applied during inversion. In addition, the seismic data gives an apparent slip gap region surrounded by the major slip patch with large slip magnitude (e.g., YE *et al.* 2015), which do not find by InSAR data inversion. Assuming 30 GPa shear modulus, the total estimated moment magnitude is $M_0 = 3.28 \times 10^{21}$ Nm, corresponding to M_w 8.3, which is comparable to GCMT or USGS solutions. The seismic rupture mainly propagated to the north and updip of the hypocenter, with almost no significant slip resolved to the south or down-dip of the hypocenter. Additionally, we find that the early aftershocks mainly occur in the regions

with low magnitudes of resolved coseismic fault slip (Fig. 1).

4. Discussion

Our geodetic inversion suggests that the rupture zone is about 400 km long and 140 km wide, sub-parallel to the western coast of South America and extending to about 30 km depth (Fig. 1). The slip mainly concentrates in an area from 40 to 100 km north of the epicenter at depth of 0–17 km, with peak thrust slip up to 8.3 m. At greater depths, slip decreases smoothly and vanishes at about 35 km depth, which is the depth of the Moho interface in Central Chile (YUAN *et al.* 2002). We also find there was a slight right-lateral component of the Illapel earthquake, which is consistent with northward motion of the Nazca plate. However, the low strike-slip component relative to the northward component of plate convergence indicates slip partitioning in the subduction system here.

Our assumption of a homogeneous elastic half-space and our constraint on rake in the inversion both have some effect on the inferred slip distribution. To assess the degree to which these assumptions influence our final slip model, in the Supplementary Material we present slip inversions assuming either a layered elastic structure or relaxing the rake constraint. While there are some differences in the inferred slip in the supplementary inversions, the main details of the inferred slip is remarkably similar. Using a layered elastic structure, the inferred slip at the trench is slightly lower (the maximum slip assuming a layered model is 12 % lower than when assuming a homogeneous half-space; Figure S1). Relaxing the rake constraint to allow for a component of left-lateral slip in the inversion still results in the thrust slip with a small component of right-lateral slip, as in the model we present in the main text.

The Southern Pacific plate subducts beneath the South American plate, with the subducted plate extending to the mantle and the plate convergence resulting in the Andean cordillera (BURKE 1988), intensive volcanoes and a large number of destructive earthquakes. The most recent earthquake ruptured just the shallow portion of the Chilean megathrust.

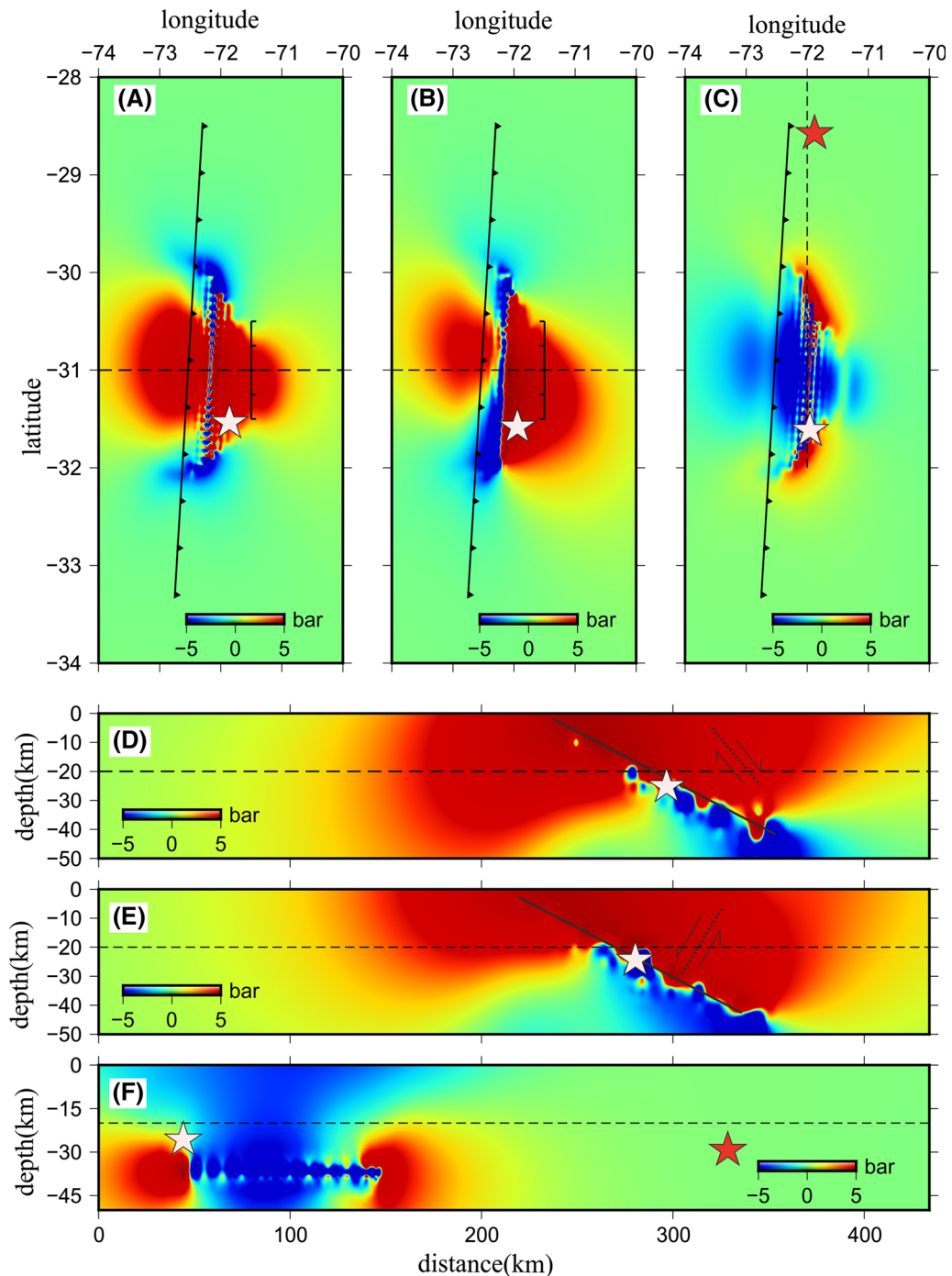
Figure 4

Coulomb stress change caused by Illapel earthquake. **a** The Coulomb stress change using receiver fault A, presented with map view at 20 km depth. *Dashed line* is a profile location shown in **d**. **b** Same with **a**, but using receiver fault B. *Dashed line* is a profile location shown in **e**. **c** Coulomb stress change using the source fault of the 1922 Mw 8.4 event as receiver fault, shown in map view at 20 km depth. *Dashed line* is the profile location shown in **f**. **d** The cross-section of the Coulomb stress change along the profile shown in **a**. *Arrows* and *short dotted line* show the dip direction and motion of the receiver fault A, respectively. The *horizontal dashed line* is the map view depth shown in **a**. **e** Same with **b** but using receiver fault B. **f** The cross-section of the Coulomb stress change along the profile shown in **c**. In all figures, the *white* and *red stars* represent the locations of the 2015 Mw 8.3 and 1922 Mw 8.4 event, respectively

We infer that the rupture started in the region between the locked and creeping zone at about 25 km depth and then propagated unilaterally up-dip and to the north.

In contrast to the Illapel earthquake, there were two separated slip patches in 2010 Mw 8.8 Maule earthquake, both to the north and south of the epicenter along the subduction interface (ARON *et al.* 2015). To the south of the Illapel epicenter, there have been two major earthquakes during the past four decades: the 1985 Algarrobo Mw 8.0 earthquake (COMTE *et al.* 1986) and the 1971 Mw 7.5 earthquake (EISENBERG *et al.* 1972). We surmise that the accumulated strain in this region was completely released during those two past earthquakes, and thus rupture did not propagate to the south of the epicenter in the Illapel earthquake. We also find that slip in the Illapel earthquake extended toward the inferred rupture boundary of the 1922 Mw 8.4 Vallenar earthquake (BECK *et al.* 1998), but did not penetrate into the slip region. This was similar to slip in the 1943 Mw 8.3 Illapel earthquake (Fig. 1), indicating that the 1922 earthquake likely released a significant amount of the accumulated strain in that region of the subduction interface.

There are many normal faults on the hanging wall of the subduction megathrust (LAURSEN *et al.* 2002; MOSCOSO *et al.* 2011), on which many Mw 4–7 normal earthquakes have been documented (MOSCOSO *et al.* 2011). Previous researchers have argued that these normal earthquakes were triggered by the large Coulomb stress change produced by megathrust earthquakes (FARIAS *et al.* 2011; LANGE *et al.* 2012;



ARON *et al.* 2015), enhanced by likely fluid presence along weakened zones of the forearc crust as evidenced by high V_p/V_s ratio (MoscOSO *et al.* 2011). However, it is interesting to note that no normal

earthquakes were observed following the Illapel earthquake. To explore the triggering effect produced by the great Illapel earthquake on possible extensional faults, we compute the Coulomb stress change

exerted by the 2015 Illapel, Chile Mw 8.3 earthquake. Calculations are performed using Coulomb 3.3 (TODA *et al.* 2005; LIN and STEIN 2004), with an effective coefficient of friction of $\mu = 0.4$, which is a typical value for subduction zones. Considering the geometry and kinematics of the normal faults (FARIAS *et al.* 2011; ARON *et al.* 2015), we calculate the Coulomb stress change for “receiver faults A” (strike 180° , dip 80° , rake -90°) and “receiver faults B” (strike 30° , dip 60° , rake -90°), corresponding to the representative normal faults. The two “receiver faults” are hypothetical faults, and we set their dips and strikes consistent with the result of ARON *et al.* (2015). Our results show the latest Chile event increases ~ 0.5 MPa Coulomb stress on both types of the receiver faults (Fig. 4), which is larger than the typical threshold value needed to trigger earthquakes (e.g., KING *et al.* 1994; LIN and STEIN 2004; HARRIS 1998; KILB *et al.* 2000). In the Supplementary Material, we show Coulomb stress changes calculated assuming either lower or higher effective friction coefficients, and while the magnitude of Coulomb stress change is affected by the assumed friction, the sign of the stress change does not vary (Figure S3). In other words, the regions we infer to be positive Coulomb stress change in these calculations are still positive for lower or higher friction. Despite that there are other complex factors in earthquake triggering, the earthquake risk of such normal faulting events in the hanging wall following the Illapel earthquake, where many populated cities are located, is most likely high.

The pattern of interseismic coupling on subduction interfaces is often used to assess where the next megathrust ruptures are likely to be. The fundamental assumption in these arguments is that the pattern of locking and coseismic slip distribution is similar (SAVAGE *et al.* 1986; BURGMANN *et al.* 2005; MURRAYET *et al.* 2006; PERFETTINI *et al.* 2010). Coseismic slip in the 2010 Mw 8.8 Maule earthquake filled in one of the gaps that was inferred to be coupled (MORENO *et al.* 2010). We find that the slip distribution of the 2015 Illapel earthquake closely correlates with the pattern of inferred interseismic coupling (MORENO *et al.* 2010). This suggests that the 2015 Illapel earthquake filled in another portion of the coupled region of the Chilean subduction interface.

Comparing the 2015 Chile megathrust earthquake rupture with earlier events is important for seismic hazard assessment. The 2015 earthquake could be a repeat of the 1943 Mw 8.3 earthquake, which coincides with the estimated recurrence interval of 83 ± 9 years in Central Chile (COMTE *et al.* 1986). If the inter-plate zone were fully locked, as proposed by KHAZARADZE and KLOTZ (2003), the slip deficit in the locked interface would be of the order of 5 m (70 years at 6.5 cm/year), which is also the average slip magnitude during the 2015 Chile earthquake. In addition, the 1943 and 2015 earthquakes have the comparable moment magnitude of Mw 8.3 (USGS 2015; BECK *et al.* 1998), and their epicenters are very close to each other (Fig. 1), lending support to the hypothesis that the Illapel earthquake is a repeat of the 1943 earthquake.

In 1997, the Punitaqui Mw 7.1 earthquake and an offshore earthquake sequence occurred in the central downdip and the northern updip segments of the 1943 rupture zone. These events partially reactivated the Coquimbo seismic gap (PARDO *et al.* 2002). However, it is interesting that none of the 1943, 1997 and 2015 events ruptured the areas of the 1922 Mw 8.4 Vallenar earthquake, and they were all limited by the rupture zone of the 1922 earthquake. It is natural the rupture of the 1943 Mw 8.3 earthquake could not propagate to the 1922 earthquake, since the accumulated strain since the 1922 Mw 8.5 Vallenar earthquake did not exceed the recurrence time interval of 83 ± 9 years (COMTE *et al.* 1986). Yet the rupture of the 2015 Mw 8.3 earthquake still did not propagate into the zone of 1922 Mw 8.5 earthquake, where the accumulated slip deficit is as high as 6 m following a slip quiescent of 93 years, just outside of the uncertainty of the 83 ± 9 years earthquake recurrence interval. There is a very slight and positive Coulomb stress change (about 0.01 MPa) on the subduction interface from the Illapel earthquake (Fig. 4), which indicates that the most recent earthquake has loaded the megathrust in the region of the 1922 earthquake, albeit to only a small degree. Even given a small Coulomb stress loading and the uncertainty in the estimated recurrence interval, the megathrust in the region of the 1922 rupture is a likely location of the next major subduction thrust earthquake on the Chilean margin, and thus the earthquake potential in this region is urgent.

5. Conclusions

The 2015 Mw 8.3 Illapel earthquake is the latest megathrust earthquake to rupture the subduction interface between the Nazca and South America plates. This latest earthquake ruptured the Coquimbo seismic gap, which has had no destructive events since Mw 8.3 earthquake in 1943. We obtain the surface deformation field of this earthquake using Sentinel-1 InSAR, which we use to estimate the coseismic slip in the Illapel earthquake. Using the estimated coseismic slip model, we calculate the resulting Coulomb stress change. Our conclusions are as follows:

1. The Illapel earthquake is a thrusting event with a slight right-lateral strike slip component. The maximum thrust-slip and right-lateral strike slip reach 8.3 and 1.5 m, respectively. The total seismic moment is 3.28×10^{21} N m, corresponding to a moment magnitude Mw 8.3.
2. The slip distribution correlates closely with the inferred interseismic coupling (MORENO *et al.* 2010), which indicates that the 2015 Illapel earthquake filled a region of accumulated strain on the shallow megathrust.
3. There is a positive Coulomb stress change caused by Illapel earthquake, favoring failure of the extensional faults in the over-riding South American plate. Though Coulomb stress change increases only slightly in the region of the 1922 megathrust earthquake, the earthquake potential in this region is urgent.

Acknowledgments

This work is co-supported by grants of Chinese National Science Foundation (41474013, 41461164002) and funding from State Key Laboratory of Earthquake Dynamics, Institute of Geology, China Earthquake Administration (LED2014A01). Sentinel SAR data is from European Space Agency. The SRTM data is downloaded from: <http://srtm.csi.cgiar.org>. Aftershocks and focal mechanisms are from USGS. Figures are generated by Generic Mapping Tools (WESSEL and SMITH 1998). Coulomb 3.3 is

used to calculate the coseismic coulomb stress changes. We thank two anonymous reviewers and the editor for comments on this manuscript.

REFERENCES

- ANGERMANN D., KLOTZ J., REIGBER C. (1999). *Space-geodetic estimation of the Nazca-south America Euler vector*. Earth planet. Sci. Lett., 171(3):329–334.
- ARON F., CEMBRANO J., ASTUDILLO F., et al (2015). *Constructing forearc architecture over megathrust seismic cycles: Geological snapshots from the Maule earthquake region, Chile*, Geological Society of America Bulletin, 127(3–4):464–479
- BARRIENTOS S.E, WARD, S.N. (1990). *The 1960 Chile earthquake: inversion for slip distribution from surface deformation*. Geophys. J. Int., 103:589–598.
- BECK S.,BARRIENTOS S.,KAUSEL E.(1998).*Source characteristic of historic earthquakes along the central Chile subduction zone*. J.S.Am.Earth Sci., 11(2):115–129
- BURKE K. (1988).*Tectonic evolution of the Caribbean*, Annu. Rev. Earth Planet. Sci., 16, 201–230.
- BURGMANN R., KOGAN M.G., STEBLOV G.M., et al(2005), *Interseismic coupling and asperity distribution along the Kamchatka subduction zone*. J.Geophys.Res., 110, B07405. doi:10.1029/2005JB003648
- CEMRANO J., LARA L.E. (2009). *The link between volcanism and tectonics in the Southern Volcanic Zone of the Chilean Andes: a review*, Tectonophysics, 471: 96–113.
- CISTERNAS M., ATWATER B.F., TORREJÓN F., et al. (2005). *Predecessors of the giant 1960 Chile earthquake*, Nature, 437, 404–407.
- COMTE A.,EISENBERG E., LORCA, et al. (1986). *The 1985 Central Chile Earthquake: A Repeat of Previous Great Earthquakes in the Region?* Science, 233:449–452
- CONTRERAS-LÓPEZ M., WINCKLER P., SEPÚLVEDA I., et al.(2016). *Field Survey of the 2015 Chile Tsunami with Emphasis on Coastal Wetland and Conservation Areas*, Pure and Applied Geophysics,173(2):349–367
- DELOUIS B., JEAN-MATHIEU N., and VALLÉE M. (2010). *Slip distribution of the February 27, 2010 Mw = 8.8 Maule Earthquake, central Chile, from static and high-rate GPS, InSAR, and broadband teleseismic data*, Geophysical Research Letters, 37, L17305. doi: 10.1029/2010GL043899,
- DE METS et al (1990).*Current plate motions*, Geophys. J. Int., 101:425–478
- EISENBERG A., HUSID R., LUCO J.E. (1972). *The July 8, 1971 Chilean earthquake*. Bull. Seismol. Soc. Am., 62(1):423–430
- FARIÁS M., COMTE D., ROECKER S., et al (2011). *Crustal extensional faulting triggered by the 2010 Chilean earthquake The Pichilemu Seismic Sequence*. Tectonics, 30(6):453–453
- FARR T G., ROSEN P A., CARO E., et al. (2000). *The Shuttle Radar Topography Mission*. Reviews of Geophysics, 45(2):37–55.
- FENG, G., and JÓNSSON S. (2012), *Shortcomings of InSAR for studying megathrust earthquakes: The case of the Mw9.0 Tohoku-Oki earthquake*, Geophys. Res. Lett., 39, L10305. doi: 10.1029/2012GL051628

- FENG G.C., LI Z.W., SHAN X.J., XU B., DU Y.N. (2015). *Source parameters of the 2014 Mw 6.1 South Napa earthquake estimated from the Sentinel 1A, COSMO-SkyMed and GPS data*, Tectonophysics. doi:10.1016/j.tecto.2015.05.018.
- HARRIS R. A. (1998). *Introduction to special section: stress triggers, stress shadows, and implications for seismic hazard*. J.Geophys.Res. 103(B10): 24347–24358
- HANSEN P. C.(1992).*Analysis of discrete ill-posed problems by means of the L-curve*,SIAM review, 34(4): 561–580.
- KHAZARADZE G., KLOTZ J. (2003). *Short- and long-term effects of GPS measured crustal deformation rates along the south central Andes*, J.Geophys.Res.108, B6. doi:10.1029/2002JB001879
- KING G.C. P., STEIN R.S., and LIN J. (1994). *Static stress changes and the triggering of earthquakes*, Bull. Seismol. Soc. Am., 84, 935–953.
- KILB D., COMBERG J., BODIN P. (2000). *Triggering of earthquake aftershocks by dynamic stresses*. Nature, 408(6812):570–574
- LANGE D., TILMANN F., BARRIENTOS S.E., et al (2012).*Aftershock seismicity of the 27 February 2010 Mw 8.8 Maule earthquake rupture zone*, Earth and Planetary Science Letters, 317–318:413–425
- LAURSEN J., SCHOLL D.W, HUENE R.V., et al (2002). *Neotectonic deformation of the central Chile margin:Deepwater forearc basin formation in response to hot spot ridge and seamount subduction*,Tectonics, 21(5), 1038. doi:10.1029/2001TC901023, 2002
- LIN, J., and STEIN R.S. (2004), *Stress triggering in thrust and subduction earthquakes and stress interaction between the southern San Andreas and nearby thrust and strike-slip faults*, J. Geophys. Res, 109, B02303. doi:10.1029/2003JB002607.
- MORENO M., ROSENAU M., ONCKEN O. (2010). *2010 Maule earthquake slip correlates with pre-seismic locking of Andean subduction zone*, Nature, 467:198–201
- MOSCOSO E., GREVEMEYER I.,REYES R.C.,et al (2011). *Revealing the deep structure and rupture plane of the 2010 Maule, Chile earthquake (Mw = 8.8) using wide angle seismic data*, Earth and Planetary Science Letters, 307,147–155
- MURRAY J., LANGBEIN, J. (2006). *Slip on the San Andreas Fault at Parkfield, California, over two earthquake cycles, and the implications for seismic hazard*. Bull. Seismol. Soc.Am. 96, 282–303
- NISHENKO,STUART P. (1985).*Seismic potential for large and great interplate earthquakes along the Chilean and Southern Peruvian Margins of South America: A quantitative reappraisal*, Journal of Geophysical Research Solid Earth, 1985, 90(B5):3589–3615
- OKADA Y. (1992). *Internal deformation due to shear and tensile fault in a half-space*, Bull. Seism. Soc. Am., 82(2), 1018–1040
- PARDO-CASAS F., MOLNAR P. (1987). *Relative motion of the Nazca (Farallon) and South American plates since late Cretaceous times*, Tectonics, 6:233–248.
- PARDO M.,COMTE D.,MONFRET T., et al (2002). *The October 15, 1997 Punitaqui earthquake (Mw = 7.1): A destructive event within the subducting Nazca plate in the Central Chile*, Tectonophysics, 345(01):199–210
- PERFETTINI H., AVOUAC J.P. TAVERA H., et al (2010). *Seismic and aseismic slip on the Central Peru megathrust*, Nature 465:78–81
- POLLITZ F.F., BROOKS B., TONG X.P., et al. (2011). *Coseismic slip distribution of the February 27, 2010 Mw 8.8 Maule, Chile earthquake*, Geophysical Research Letters, 38:L09309. doi:10.1029/2011GL047065
- SAVAGE J. C., LISOWSKI M. & PRESCOTT W. H. (1986), *Strain accumulation in the Shumagin and Yakataga seismic gaps, Alaska*.Science 231:585–587
- SIMONS M., FIALKO Y., RIVERA L. (2002). *Coseismic Deformation from the 1999 Mw 7.1 Hector Mine, California, Earthquake as Inferred from InSAR and GPS Observations*, Bull. Seismol. Soc. Am., 92, 1390–1402.
- SOMOZA R. (1998). *Updated Nazca (Farallon)-South America relative motions during the last 40 My: implications for the mountain building in the central Andean region*. J. S. Am. Earth Sci., 11:211–215.
- TONG X.P., SANDWELL D., and LUTTRELL K., et al (2010).*The 2010 Maule, Chile earthquake: Downdip rupture limit revealed by space geodesy*, Geophysical Research Letters, 37, L24311
- TODA S., R. S. STEIN, K. RICHARDS-DINGER, et al (2005). *Forecasting the evolution of seismicity in southern California: Animations built on earthquake stress transfer*, Journal of Geophysical Research, v. 110, B05S16. doi:10.1029/2004JB003415.
- VIGNY C., SOCQUET A., PEYRAT S., et al (2011). *The 2010 Mw 8.8 Maule Megathrust Earthquake of Central Chile, Monitored by GPS*. Science, 332(17):1417–1421
- WANG R.J, MARTÍN F.L., ROTH F. (2003). *Computation of deformation induced by earthquakes in a multi-layered elastic crust—FORTRAN programs EDGRN/EDCMP*. Computers & Geosciences, 29(2):195–207
- WATT S.F.L., PYLE D.M., MATHER T.A. (2009). *The influence of great earthquakes on volcanic eruption rate along the Chilean subduction zone*, Earth planet. Sci. Lett., 277:399–407.
- WEGMÜLLER U. & WERNER C.L. (1997). Gamma SAR processor and interferometry software, in proceeding of the 3rd ERS Symposium, Eur. Space Agency Spec. Publ., ESA SP-414, 1686–1692.
- WESSEL P., SMITH W.H.F.(1998), *new, improved version of the Generic Mapping Tools released*, Eos Transactions American Geophysical Union, 1998, 79(47),579–579
- WERNER C.,WEGMULLER U.,STROZZI T.,WIESMANN A.(2002).Processing strategies for phase unwrapping for InSAR applications, in Proceedings of the EUSAR 2002, Cologne, 2002 June 4–6.
- YE L.L., LAY T., KANAMORI H., et al. (2015). *Rapidly Estimated Seismic Source Parameters for the 16 September 2015 Illapel, Chile Mw 8.3 Earthquake*. Pure Appl. Geophys. doi:10.1007/s00024-015-1202-y
- YUAN X., SOBOLEV S.V., KIND R. (2002).*Moho topography in the central Andes and its geodynamic implications*. Earth planet. Sci. Lett., 199 (3-4):389–402.
- ZHANG G. H., QU C.Y., SHAN X.J., et al (2011). *Slip distribution of the 2008 Wenchuan Ms 7.9 earthquake by joint inversion from GPS and InSAR measurements: A resolution test study*, Geophys. J. Int., 186, 207–220. doi:10.1111/j.1365-246X.2011.05039.x.